Agricultural and Forest Meteorology 301-302 (2021) 108356

Contents lists available at ScienceDirect

Agricultural and Forest Meteorology

journal homepage: www.elsevier.com/locate/agrformet

Importance of calibration in determining forest stand transpiration using the thermal dissipation method

Naoya Fujime [a,*], Tomo'omi Kumagai [a,b,c], Tomohiro Egusa [a], Hiroki Momiyama [a], Yoshimi Uchiyama [d]

[a] Graduate School of Agricultural and Life Sciences, The University of Tokyo, 1-1-1 Yayoi, Bunkyo-ku, Tokyo 113-8657, Japan
[b] Institute for Space-Earth Environmental Research, Nagoya University, Furo-cho, Chikusa-ku, Nagoya 464-8601, Japan
[c] Water Resources Research Center, University of Hawai'i at Mānoa, 2540 Dole Street, Honolulu, HI 96822, USA
[d] Kanagawa Prefecture Natural Environment Conservation Center, 657 Nanasawa, Atsugi, Kanagawa 243-0121, Japan

ARTICLE INFO

Keywords:
Granier-type sensor
Evapotranspiration
Sap flux
Plant water use
Plant hydraulics
Error analyses

ABSTRACT

Forest transpiration (T_r) is the major hydrologic flux from terrestrial ecosystems; it dominates the catchment water budget and land surface energy balance and can be used as an index of exchange efficiency between vegetation and the atmosphere. The thermal dissipation method (TDM) is used to obtain the xylem sap flux density (F_d) of individual tree stems; it is among the most powerful tools for estimating forest stand T_r (T_{r_stand}) values. Individual tree T_r values can be upscaled to T_{r_stand} as a product of stand total sapwood area (A_{S_stand}) and stand mean F_d (J_S). In this study, we performed laboratory experiments using Japanese cedar (*Cryptomeria japonica* D. Don) to examine errors in T_{r_stand} values generated by mis-estimation of A_{S_stand} and/or J_S. We found that simple color identification of the stem hydroactive zone in sapwood and heartwood had little effect on accurate estimation of A_{S_stand} values. Then we examined the effects of mis-estimation of J_S, which is primarily the result of F_d measurement failures. Considering that uncertainties in heat-tracer-derived F_d values using the TDM have been identified in numerous previous studies, we applied calibration to improve the accuracy of TDM-F_d derivation using freshly cut sapwood segments of sample Japanese cedar stems and negative pressure as a driving force to determine F_d within the segments experimentally. The calibration experiment revealed that the calibrated conversion equation for heat-tracer-derived F_d values resulted in values that differed significantly from those determined using the original TDM equation and significant underestimation of T_{r_stand}. The F_d correction increased the annual T_{r_stand} value from 229 to 593 mm year^{-1}, while the corrected value was not significantly different from the T_{r_stand} value obtained from catchment-scale water budget observations. The novel TDM calibration equation improved TDM-based T_{r_stand} estimates dramatically, highlighting the importance of this study's calibration method.

1. Introduction

Forest transpiration (T_r) is the major hydrologic flux from terrestrial ecosystems; it dominates the catchment water budget and land surface energy balance, and can be used as an index of the efficiency of exchange of some materials between vegetation and the atmosphere (Jasechko et al. 2013). Heat-based sapflow measurements are the most common approach for assessing the environmental control of individual-scale T_r and quantifying stand-scale T_r (T_{r_stand}) due to their low cost, ease of equipment installation, and long-term measurement period (Poyatos et al. 2016). Sapflow methods are used to measure the entire sapflow or xylem sap flux density (F_d) through a conductive area by tracking convective heat transport promoted by sapflow (Poyatos et al. 2016); these methods include the thermal dissipation method (TDM; Granier 1987), and the heat pulse velocity (Marshall 1958), heat ratio (Burgess et al. 2001), heat field deformation (Nadezhdina et al. 2012), and stem heat balance methods (Čermák et al. 1973).

The TDM to obtain F_d is by far the most commonly used heat-based sapflow measurement method (Poyatos et al. 2016, Peters et al. 2018), and it has been applied to investigate T_r at the stand, catchment, and landscape scales (Mackay et al. 2002, Pataki and Oren 2003, Ewers et al. 2005, Kumagai et al. 2005*a*, 2007, 2008, 2014, Bladon et al. 2006, Sun

* Corresponding author.
E-mail address: naoyafujime@gmail.com (N. Fujime).

https://doi.org/10.1016/j.agrformet.2021.108356
Received 18 August 2020; Received in revised form 6 February 2021; Accepted 7 February 2021
Available online 20 February 2021

et al. 2014). In the TDM, scaling procedures are required to extrapolate to ground area-based T_{r_stand} values (Kumagai et al. 2008) as follows:

$$T_{r\_stand} = J_S \frac{A_{S\_stand}}{A_G} \quad (1)$$

where J_S is the stand mean F_d, A_{S_stand} is the stand total sapwood area, and A_G is the stand ground area. Two major sources of error must be accounted for in T_{r_stand} estimates, i.e., determining J_S and A_{S_stand} (Kumagai et al. 2005*a*, *b*).

A_{S_stand} is generally estimated by integrating all individual tree sapwood area estimates (A_{S_tree}) in the stand, species-specific allometric equations describing the relationship between the stem diameter at breast height (DBH) and A_{S_tree} are used for this purpose (e.g., Wullschleger et al. 2001). Our previous study (Kumagai et al. 2005*b*) determined the appropriate amount of allometric data (DBH and A_{S_tree}) for derivation of the allometric equation. In conventional estimation of the A_{S_tree} value of each sample tree, color difference is used to identify the boundary between sapwood and heartwood, and the thickness of the detected sapwood is measured using a ruler. Thus, the precision of A_{S_tree} estimates remains problematic for A_{S_stand} estimation.

Evaluations of tree-to-tree and within-tree variation in F_d are the most important considerations in obtaining the appropriate J_S. Kumagai et al. (2005*a*) proposed sampling strategies in terms of how many sample trees and radial depths were required for F_d measurement to estimate the representative J_S for a stand. T_{r_stand} scaled from TDM-F_d measurements often underestimates eddy covariance (EC)-derived water vapor flux, which can approximate to actual T_{r_stand} under ideal conditions, e.g., simple terrain and spatial vegetation homogeneity or an appropriate EC footprint (Oishi et al. 2008). Further comparisons between TDM and EC measurements conducted at the same site (e.g., Kumagai et al. 2014, Shimizu et al. 2015) could provide strong evidence of TDM underestimation of EC values. Although discrepancies between the TDM and EC measurements may simply be due to shortcomings of both methods, many recent laboratory experiments have demonstrated that the original conversion equation for F_d from heat tracers in the TDM results in consistent underestimation of actual F_d values, whereas novel species-specific parameters in the conversion equation substantially improve the accuracy of TDM-based measurements (Steppe et al. 2010, Sun et al. 2012, Paudel et al. 2013, Fuchs et al. 2017, Peters et al. 2018, Flo et al., 2019). Nonetheless, few studies have adopted species-specific calibration of TDM-F_d derivation as a best practice for accurately estimating T_{r_stand} (e.g., Herbst et al. 2008, Ma et al. 2017); furthermore, to our best knowledge, no study has validated T_{r_stand} values estimated by calibrated TDM measurements using independent forest water use observations such as EC and soil water balance measurements.

In this study, we obtained satisfactory quantification of T_{r_stand} values using TDM measurements. We investigated how precisely A_{S_tree} values can be detected for trees within a stand, how J_S can be properly estimated, and which factors in the implementation of the TDM are influential in estimating T_{r_stand}. Like previous studies (e.g., Peters et al. 2018), we suspected that the conversion equation to derive F_d values from heat-tracer measurements would be the major cause of mis-estimation of J_S and resultant T_{r_stand} values. Therefore, we performed calibration experiments using freshly cut sapwood segments from sample stems and artificial F_d for these segments in the laboratory to derive novel species-specific parameters for the conversion equation, and corrected the TDM-based T_{r_stand} values measured in a forested catchment using the calibrated conversion equation. Then we validated the corrected T_{r_stand} data using catchment-scale water budget observations, which is the main novel contribution of this investigation.

2. Materials and methods

2.1. Study site and field observations

This study was conducted in the Oborasawa Experimental Watershed (OEW), a 55-ha forest headwater catchment in the Kanto region of Japan (Suppl. Material Fig. S1; 35°28'N, 139°12'E, 432–878 m a.s.l.). The catchment is located in a mountainous area with a slope (mean ± standard deviation [SD]) of 34.9° ± 9.0° and is underlain by tuff and tuff breccia of Neogene age. The soil is classified as Cambisol and the average soil depth is 1.64 m. Forest in the OEW consists mainly of coniferous plantation stands, i.e., *Cryptomeria japonica* D. Don and to a lesser extent, *Chamaecyparis obtusa* Endl. with fragmented deciduous broadleaved trees (e.g., *Cercidiphyllum japonicum* Sieb. et Zucc. and *Aesculus turbinata* Blume). The mean annual precipitation (P_r) for the period 2010–2017 was 2952.6 mm, with the rainy season occurring from mid-June to early July. The mean annual air temperature (T_a) was 12.3°C in 2010–2017. In 2018, the annual T_a was 13.6°C, with a minimum mean daily T_a of −3.6°C in January and a maximum mean daily T_a of 28.9°C in August. The mean daily vapor pressure deficit (VPD), averaged over daylight hours (06:00–18:00 LT), reached a maximum of 1.5 kPa in May 2018. Further description of the site has been presented elsewhere (Oda et al. 2013, Egusa et al. 2019).

A 48-ha subcatchment (No. 1) of the OEW was devoted to catchment-scale water budget observations; the discharge (Q) from catchment No. 1 was observed using a V-notch weir. An even-aged 30-year-old *Cr. japonica* stand plot (297 m^2) on a downward slope from the ridge in catchment No. 1 was selected for sapflow and canopy-interception (I_C) measurements. The measurement plot was 370 m from the weir and the mean slope of the plot was 27.8°. The number of trees, mean DBH (SD), and mean tree height (SD) at the measurement plot were 38, 26.5 (4.3) cm, and 20.1 (2.3) m, respectively. The leaf area index (LAI) at the measurement plot was measured five times in 2018 using a plant canopy analyzer (LAI-2000, Li-Cor, Lincoln, NE, USA), and the mean LAI was 3.7. Tree stems used for the laboratory calibration experiments were sampled at a *Cr. japonica* stand adjacent to the measurement plot. The number of trees used for sap flux onsite measurements, sapwood analyses, and laboratory measurements was 16, 16, and 5, respectively.

Meteorological conditions were observed in an open field on the ridge of catchment No. 1 and close to the measurement plot; P_r was measured using a tipping-bucket rain gauge (N78, Nippon Electric Instrument Inc., Tokyo, Japan) and calibrated using a storage-type rain gauge. A pyranometer (LP PYRA 03, Delta Ohm, Caselle di Selvazzano, Italy) was installed at the top of an 18-m tower in the open field to observe incident radiation (R_s). A T_a and relative humidity probe (HMP155, Vaisala, Helsinki, Finland) was installed at the same height as the pyranometer on the tower to calculate VPD at canopy height.

2.2. Sapflow measurements and sapwood analyses

Custom-made Granier-type TDM sensors (Granier, 1987) were used to measure F_d in the field and laboratory. Each sensor consists of a pair of probes (length, 20 mm; diameter, 2 mm). The probes were inserted into the sapwood approximately 0.15 m apart. The upper probe, which includes a heater, was supplied with 0.2 W constant power. The heat was dissipated into the sapwood and vertical sap flux surrounding the probe. Then the temperature difference between the upper heated probe and the lower unheated reference probe (ΔT: K) was measured and converted into F_d ($m^3\ m^{-2}\ s^{-1}$) according to Granier (1987):

$$F_d = \alpha K^{\beta} \quad (2)$$

in which

$$K = \frac{\Delta T_{max} - \Delta T}{\Delta T} \quad (3)$$

where α ($m^3\ m^{-2}\ s^{-1}$) and β are fitted parameters empirically determined by Granier (1987) to be 1.19×10^{-4} $m^3\ m^{-2}\ s^{-1}$ and 1.231, respectively; K is the dimensionless flux index, and ΔT_{max} (K) is the maximum ΔT, which can be obtained under zero-flow conditions.

At the measurement plot, 16 trees were selected for F_d measurements, such that the number of trees measured in each DBH class corresponded to the DBH frequency distribution in the plot (Kumagai et al. 2007). The DBH frequency distribution in the measurement plot is shown in Suppl. Material Fig. S2. Two sensors were inserted into each selected tree to a depth of 0–20 mm on the northeast- and southwest-facing sides in consideration of the azimuthal variation in F_d. Mobile sensors (Delzon et al. 2004, Tateishi et al. 2010) were placed on the northwest-facing sides of all selected trees to measure F_d at four (0–20, 10–30, 20–40, and 30–50 mm) depths for each tree to ensure coverage of the hydroactive xylem. We derived the radial F_d profile from the mobile sensor measurements following a previously published protocol (Tateishi et al. 2010). The F_d signals, i.e., ΔT, were saved using a data logger (CR10X, Campbell Scientific Inc., Logan, UT, USA) with a multiplexer (AM16/32, Campbell Scientific Inc.) every 30 s and averaged over 30 min. For this investigation, we used the 2018 observation data.

Sapwood thickness (mm) in a core extracted with a 5-mm increment borer at about breast height from each selected tree was measured using a ruler, and assessed based on the mean of two orthogonal measurements (Suppl. Material Fig. S3). Assuming that the stem cross-sections were circular, A_{S_tree} was obtained as the difference between the stem cross-sectional area beneath the bark and the stem cross-sectional heartwood area. An allometric equation describing the relationship between DBH and A_{S_tree} based on available allometric data allowed us to estimate A_{S_stand} by applying the equation to all 38 trees in the measurement plot.

In *Cr. japonica*, distinct color differences are used to identify the boundary between sapwood and heartwood. Because *Cr. japonica* has an unclear transition zone between sapwood and heartwood, i.e., the 'white zone' (Nobuchi and Harada 1983, Nakada et al. 1999), where moisture content is much lower than in heartwood, and which is impervious to water, it is necessary to subtract the white-zone thickness from the apparent sapwood thickness to estimate the hydroactive area of the stem. However, the white zone is only slightly lighter than actual sapwood; thus, these areas are difficult to distinguish, which may be a potential source of error in A_{S_stand} estimates. Therefore, we compared the apparent sapwood area with the actual sapwood area determined in the laboratory by examining all core samples from the plot, after dying with a 0.1% acid fuchsin solution. Regarding the relationship between DBH and sapwood thickness, i.e., hydroactive-zone width, analysis of covariance (ANCOVA) confirmed that the difference between the sapwood thickness derived from the laboratory experiment and the thickness estimated based on distinct color differences was not statistically significant ($p = 0.29$, based on 16 sample trees). Therefore, we did not consider the effects of this potential error on A_{S_stand} values in subsequent error analyses. The linear function of DBH (m) was fitted to A_{S_tree} (m^2) in the measurement plot ($A_{S\_tree} = 0.16$ DBH $- 0.018$, $R^2 = 0.88$) (Suppl. Material Fig. S4). We applied this equation to the DBH of 38 trees in the measurement plot and calculated an A_{S_stand} value of 0.95 m^2.

2.3. Upscaling and error analyses

The F_d value of each measured tree i (F_{di}) was scaled up to T_{r_stand} ($m^3\ m^{-2}\ s^{-1}$) using Eq. (1), such that J_S ($m^3\ m^{-2}\ s^{-1}$) was formulated as:

$$J_S = \frac{J_{S1}\sum_{i=1}^{n}A_{1i} + J_{S2}\sum_{i=1}^{n}A_{2i}}{\sum_{i=1}^{n}A_{1i} + \sum_{i=1}^{n}A_{2i}} = J_{S1}f_p \quad (4)$$

in which

$$f_p = \frac{\sum_{i=1}^{n}A_{1i} + \frac{J_{S2}}{J_{S1}}\sum_{i=1}^{n}A_{2i}}{\sum_{i=1}^{n}A_{1i} + \sum_{i=1}^{n}A_{2i}} \quad (5)$$

where n is the number of measured trees; J_{S1} and J_{S2} are the J_S values for all measured trees at 0–20 and 20–40 mm, respectively; A_{1i} and A_{2i} are the sapwood areas (m^2) for xylem bands at 0–20 and 20–40 mm, respectively; and f_p is a measure of the radial variation in F_d values for the whole plot, and varies between $(\sum_{i=1}^{n}A_{1i})/(\sum_{i=1}^{n}A_{1i} + \sum_{i=1}^{n}A_{2i})$ (for no J_S at 20–40 mm) and 1 (for $J_{S2} = J_{S1}$, which reflects the equal J_S between 20–40 mm and the outer 20 mm of the xylem). Using Eq. (2), J_{S1} was given by:

$$J_{S1} = \frac{\sum_{i=1}^{n}F_{di}A_{1i}}{\sum_{i=1}^{n}A_{1i}} = \frac{\sum_{i=1}^{n}\alpha K_i^{\beta}A_{1i}}{\sum_{i=1}^{n}A_{1i}} \quad (6)$$

Eqs. (4) and (6) were combined with Eq. (1) to give:

$$T_{r\_stand} = \frac{\sum_{i=1}^{n}\alpha K_i^{\beta}A_{1i}}{\sum_{i=1}^{n}A_{1i}} f_p \frac{A_{S\_stand}}{A_G} \quad (7)$$

where A_{S_stand} and A_G are expressed in m^2.

Any detailed examination of potential for accurate forest water use estimates in a catchment must address which parameter is the strongest determinant of T_{r_stand} values. In a previous study, we took into consideration the effect of the sample size used for J_S and A_{S_stand} estimates on the error associated with T_{r_stand} estimation (Kumagai et al. 2005*a*, *b*); notably, measuring azimuthal variation in F_d did not improve the accuracy of T_{r_stand} estimates (Komatsu et al. 2016). Thus, we assumed that the error in T_{r_stand} (dT_{r_stand}/T_{r_stand}) was associated with species-specific parameters in the K–F_d conversion equation (Eq. (2)), α and β and the radial F_d variation index, f_p ($d\alpha/T_{r\_stand}$, $d\beta/T_{r\_stand}$, and df_p/T_{r_stand}, respectively), and that tree-to-tree variation in $\ln K_i$ (where i = 1, 2, ⋯, n) was sufficiently small, i.e., $\ln\overline{K_i} \approx \ln K_i$ (where the overbar denotes the ensemble average). Considering only the first-order terms of the total derivative expansions in Eq. (7) results in the following expression (e.g., Igarashi et al. 2015):

$$\frac{dT_{r\_stand}}{T_{r\_stand}} = \frac{1}{T_{r\_stand}}\left(\frac{\partial T_{r\_stand}}{\partial \alpha}d\alpha + \frac{\partial T_{r\_stand}}{\partial \beta}d\beta + \frac{\partial T_{r\_stand}}{\partial f_p}df_p\right) = \frac{d\alpha}{\alpha} + \left(\ln\overline{K_i}\right)d\beta + \frac{df_p}{f_p} \quad (8)$$

where the first, second, and third terms on the right side of the equation represent the contributions of errors in α, β, and f_p, respectively, to error in T_{r_stand} values.

2.4. Laboratory calibration experiments

Laboratory calibration experiments were performed on the hydroactive area, i.e., partial area of sapwood in *Cr. japonica* tree stems, following the method of Iida et al. (2020) with some modifications (Fig. 1). In November 2018, five trees were logged, and 17 cut sapwood segments were extracted from the stems at the breast height of the sampled trees (Fig. 1a). The sides of the cut sapwood segments were sealed with a silicon sealant to prevent air entry into the segment from the sides, and a set of TDM probes was inserted into the sapwood. The cut sapwood segments were recut at the lower end under water, resulting in a segment size of 4.0 cm × 4.0 cm × 50.0 cm, and immersed in 20 mM KCl solution to reduce hydraulic resistance (Zwieniecki et al. 2001).

A polyvinyl chloride (PVC) cap with a rubber clamp and a connector was attached to the upper end of a cut segment and connected via flexible tubing to an artificial F_d generation system that consisted of a vacuum pump (DAS-01, AS ONE, Osaka, Japan), an Erlenmeyer flask, and a pressure regulator (CVC3000, VACUUBRAND, Wertheim,

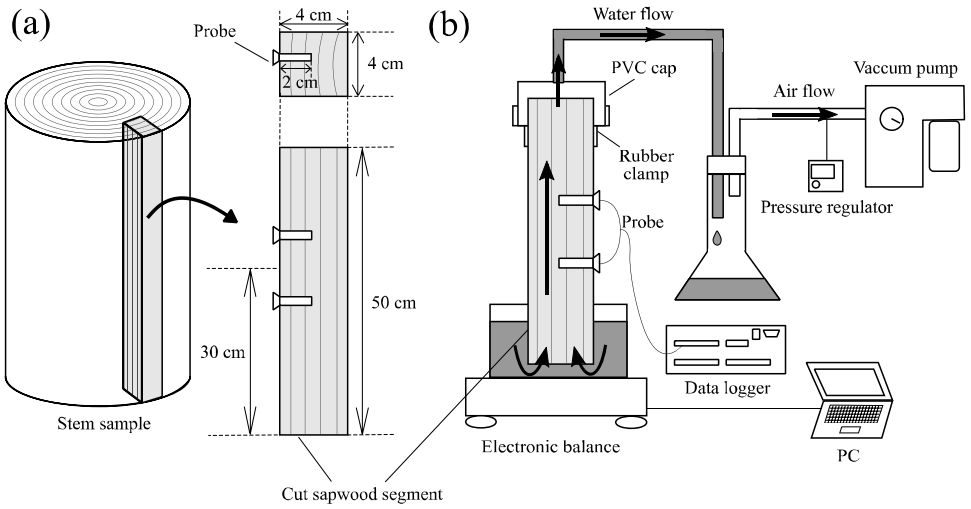

Fig. 1. Schematic diagram of the calibration experiment system used to derive novel species-specific parameters for the conversion equation for sap flux density (F_d) from a heat tracer. (a) A freshly cut sapwood segment extracted from a stem sample. (b) System for generating artificial F_d within the cut sapwood segment using negative pressure as a driving force.

Germany) (Fig. 1b). The amount of KCl solution flowing out from the segment was gravimetrically measured using an electronic balance with 0.01-g resolution (GX-8K, A&D Company, Tokyo, Japan) and recorded on a computer at 1-min intervals. TDM sensor signals, ΔT, were recorded on a data logger (CR10X) every 1 min.

For each cut sapwood segment, the relationships between F_d and K were measured at four negative pressures (200, 400, 600, and 800 hPa) generated by the vacuum pump to obtain novel species-specific parameters, i.e., α and β in the K–F_d conversion equation (Eq. (2)). At each pressure, the stationary state for K and F_d was obtained over 60 min, and analysis values were obtained during the 30-min period thereafter. After completion of all four pressure stages, the vacuum pump was stopped to reset the pressure to atmospheric pressure, and then ΔT_{max} was obtained under the zero flux condition. Immediately following the measurement of each segment, we passed 0.1% acid fuchsin solution through the segment for 90 min and collected the dyed cross-section at the heating probe. Thus, the hydroactive area was precisely measured on the dyed sapwood portion, and F_d was obtained by dividing the amount of KCl solution that passed through the segment by the hydroactive area.

2.5. Catchment-scale transpiration estimation

Catchment-scale water budget observations can be used to derive evapotranspiration (ET) averaged over the catchment, which is equivalent to $T_r + I_C$ at the catchment or stand scale. Thus, for the T_{r_stand} estimate using catchment-scale water budget observations, not only the ET estimate but also I_C observations and the subtraction of I_C from ET are required.

Given that there is little bedrock drainage in the OEW (Oda et al. 2013) and that Q is a function of soil water storage, ET during the specific hydrological period t_1 to t_2 can be expressed using the short-term water budget method (STWB; Linsley et al. 1958, Suzuki 1985, Momiyama et al. 2019) as follows:

$$\mathrm{ET} = \int_{t_1}^{t_2} p_r(t)\mathrm{d}t - \int_{t_1}^{t_2} q(t)\mathrm{d}t \tag{9}$$

where ET is the total amount of ET (mm) in the specific hydrological period, t is the time (days), p_r is the daily P_r rate (mm day^{-1}), and q is the daily Q rate (mm day^{-1}). Daily values, p_r and q, of the data obtained in 2010–2017 were used for this analysis, because the weir was buried by sediment and the Q could not be measured between January and July 2018. The start and end dates of the specific hydrological period, i.e., t_1 and t_2, respectively, were determined using the following criteria: no p_r on those dates or during the previous 2 days, the difference in q between t_1 and t_2 was within 5% of q at t_1, the period was longer than 8 days and shorter than 85 days, and P_r during the period was greater than 30 mm. ET (mm) obtained in the specific hydrological period was divided by its duration (days), resulting in daily ET (mm day^{-1}). We arranged the daily ET to obtain monthly mean daily values.

Stemflow (SF) and throughfall (TF) were obtained in the measurement plot as follows. Collars placed around the trunks were connected to PE plastic bottles, allowing SF measurements on six trees in the plot. We placed 19 PE plastic bottles with a 21-cm diameter funnel on the forest floor to collect TF, and the weight of the bottles was measured using a scale (Model 393-50, Custom Corporation, Tokyo, Japan). SF and TF were measured at intervals of 1 to several weeks including single to several storm events. Linear regression equations obtained the relationships between P_r and SF (slope = 0.04; R^2 = 0.87) and P_r and TF (slope = 0.82; R^2 = 0.99). Thus, the ratios of SF to P_r (SF/P_r) and TF to P_r (TF/P_r) were calculated, along with the ratio of I_C to P_r (I_C/P_r). The I_C/P_r ratio was 0.14 at the plot in 2018. Hence, monthly mean daily I_C (mm day^{-1}) in 2010–2017 was estimated to be a product of I_C/P_r and the 2010–2017 monthly mean p_r, allowing us to estimate the 2010–2017 monthly mean daily T_{r_stand} (mm day^{-1}).

Note that STWB has several assumptions, which can affect the calculation results. First, we assumed that the effect of forest floor evaporation was negligible, and that there was no seasonality in the I_C/P_r ratio. When LAI exceeds 3, it was assumed that forest floor evaporation had a smaller effect on ET compared to the T_r (Kelliher et al. 1995). At the measurement plot, the LAI was 3.7, i.e., far higher than 3. Regarding the relationships between P_r and SF and between P_r and TF, ANCOVA confirmed that the difference between summer (May–October) and winter (November–April) was not statistically significant (p = 0.60 and 0.40, respectively). Therefore, our assumptions regarding ET can be considered valid. Next, we assumed that P_r would immediately contribute to water storage in the catchment. In this catchment, it snows during the winter. The time lag between snow accumulation and snowmelt can affect the results of the STWB; this will be discussed in the Results section. Finally, we assumed that the amount of water stored in the catchment corresponds to the Q. However, the time-series changes in surface soil moisture may deviate from the time-series changes in Q (Brooks et al. 2010). We investigated this based on soil moisture observations. Volumetric water content was measured by water content reflectometers (CS616; Campbell Scientific Inc.) at 10, 30, and 70 cm

depths in the measurement plot. The values measured at each depth were considered to represent 0–20, 20–50, and 50–90 cm, respectively. The amount of soil moisture up to a depth of 90 cm was calculated, and the changes of soil moisture (ΔS) during the period t_1 to t_2, selected by the same criteria as for STWB, was obtained. For the analysis, the data from August 2018 to July 2019 were used, when both the Q and volumetric water content were measured. It was confirmed that the monthly mean ΔS did not exceed 0.1 mm, and the effect of soil moisture on the surface layer on the result of the STWB can be ignored.

3. Results

3.1. Novel species-specific calibration curve

The calibration curve with novel species-specific parameters in the K–F_d conversion equation, which was obtained from the cut-sapwood experiments ($R^2 = 0.49$), was appreciably different from the original Granier (1987) calibration curve (Fig. 2). The parameters α and β in Eq. (2), determined experimentally, were 2.73×10^{-5} and 0.371, respectively. The 95% confidence interval for α ranged from 1.91×10^{-5} to 3.97×10^{-5}, and for β it ranged from 0.253 to 0.509. The novel calibration curve had a gentler slope and lower F_d values in the higher K domain than the original Granier curve because both parameters were lower than those proposed by Granier ($\alpha = 1.19 \times 10^{-4}$, $\beta = 1.231$). This discrepancy resulted in overall underestimation of actual F_d values by the original Granier curve despite possible underestimation by the novel calibration curve under higher F_d conditions. Such higher F_d conditions were rare in the field (<5% of all events; Fig. 2).

We also found a significant decrease in β with decreasing K_{min}, which was a minimum value of the K used for each previous calibration experiment (Suppl. Material Table S1; Fig. 3). Only data obtained under negative pressure as a driving force for experimental F_d were used for this analysis. The mean (SD) values of α, β, and K_{min} used in this analysis were 7.01×10^{-3} (1.53×10^{-2}), 1.29 (0.382), and 3.10×10^{-2} (3.42×10^{-2}), respectively. The linear regression line is shown in Fig. 3 ($\beta = 0.32 \log_{10} K_{min} + 1.91$; $R^2 = 0.46$, $p < 0.005$). This finding implies that the experimental design, i.e., the range of K used in the calibration experiments, may determine the shape of the calibration curve (i.e., β), and that the reason β was smaller in this study than in previous experiments may be because the second smallest K_{min} in those experiments was adopted in the present experiment.

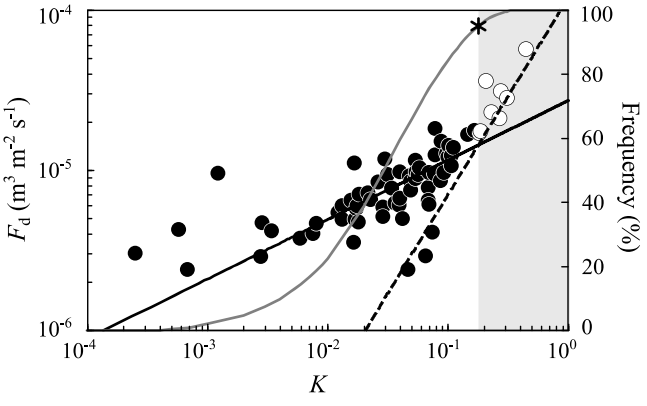

Fig. 2. Calibration curves to derive sap flux density (F_d) from the dimensionless flux index representing heat tracer movement (K) obtained from cut sapwood segment experiments (black solid line) and the original Granier equation (1987) (dotted line). Gray solid line represents the cumulative frequency of K measured in the field; gray area and asterisk represent upper 5% area of K values in the frequency. Circles indicate data obtained from cut sapwood segment experiments; open circles indicate data within the 5% area.

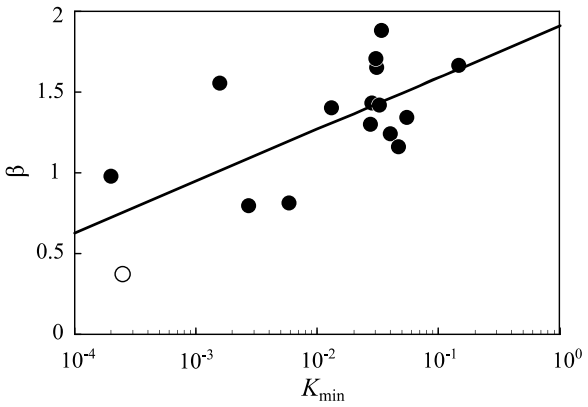

Fig. 3. Relationship between minimum values of the dimensionless flux index representing heat tracer movement, K (K_{min}), in the calibration experiments performed in this study (open circle) and the literature (closed circles; Table S1 at Suppl. Material), and the fitted parameter (β) in the K–sap flux density (F_d) conversion equation (Eq. (2)).

3.2. Error analyses

Using the original Granier curve, F_d values for the innermost sapwood were almost half those of the outermost sapwood, whereas using the novel calibration, F_d values for the outermost sapwood decreased by only ca. 20% relative to the innermost sapwood (Fig. 4); we emphasize that our dye solution experiments confirmed the innermost sapwood depth. Overall, using the novel calibration curve, the decrease in F_d with increasing sapwood depth became gradual due to enhanced F_d under lower F_d conditions (Figs. 2 and 4).

The size of the increments in Eq. (8) was defined as the difference between the values adopted by the novel calibration curve and those of the original Granier curve for dα and dβ (Fig. 2), and the difference between values assuming constant F_d along the sapwood depth and actual radial variation in F_d when adopting the novel calibration curve for df_p (Fig. 4). First-order error analyses (Eq. (8)) revealed the relative importance of each variable (i.e., α, β, and f_p) in the error in the T_{r_stand} estimate, dT_{r_stand}/T_{r_stand} (Fig. 5). The significance of each variable for dT_{r_stand}/T_{r_stand} was in the order $\beta \geq \alpha \gg f_p$. Notably, any error in the f_p estimate (see Eq. (5)) would be attributed to failure to detect radial variation in F_d rather than hydroactive sapwood area. If the original Granier curve was used to estimate the radial profile of F_d, df_p the resulting dT_{r_stand}/T_{r_stand} would become greater (see Fig. 4). In other words, the major cause of error in f_p estimates may be the effect of using the original Granier curve; thus, the impact of α and β on dT_{r_stand}/T_{r_stand}

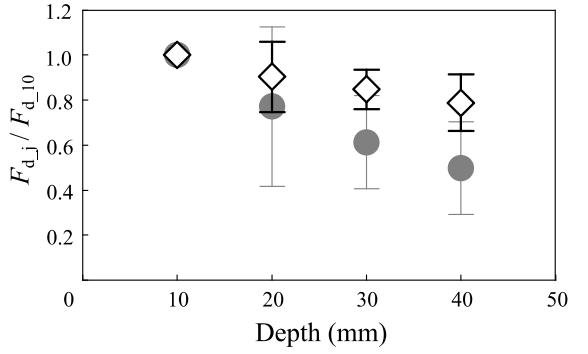

Fig. 4. Radial profile of sap flux (F_d) ratio (F_{d_j}/F_{d_10}, where F_{d_j} and F_{d_10} are F_d values at depths of j and 10 mm beneath the bark, respectively) as a function of depth j in stems of measured trees. Diamonds and closed circles indicate values calculated by the novel calibration equation and the original Granier equation, respectively. Vertical bars indicate standard deviation (SD).

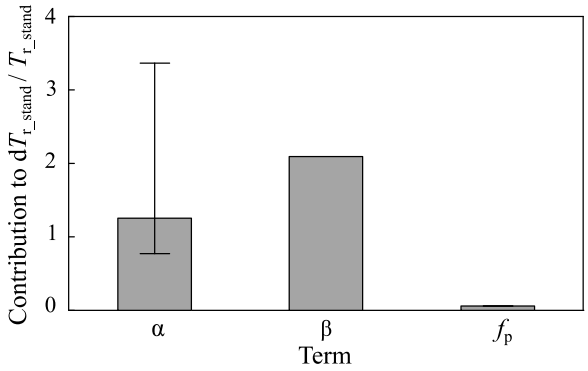

Fig. 5. Contributions of the first (α), second (β) and third (f_p) terms in Eq. (8) to error in the stand transpiration (T_{r_stand}) estimate (dT_{r_stand}/T_{r_stand}). α, β, and f_p are defined in the text. Error bars indicate the maximum and minimum possible contributions.

may be more critical than shown by the present analyses.

3.3. Yearly stand-scale transpiration

Monthly mean diurnal cycles of J_S calculated using the novel species-specific calibration equation and the original Granier calibration equation were compared in May and December, when monthly mean daily T_{r_stand} values were highest and lowest, respectively, in 2018 (Fig. 6). In the low F_d domain, the novel calibration equation resulted in higher F_d values than did the original equation (Fig. 2). Therefore, when using the novel calibration equation, an increase in J_S was more appreciable at night than during the daytime in both May and December (Fig. 6). Furthermore, the monthly mean daily T_{r_stand} values using the original and novel equations were 1.2 and 2.3 mm day^{-1}, respectively, in May and 0.3 and 1.6 mm day^{-1}, respectively, in December. In short, the rate of increase of T_{r_stand} calculated using the novel equation compared to that calculated using the original equation was 5.3 in December (i.e., mid-dormant season), which was much greater than the value of 1.9 obtained in May (i.e., early growing season).

We also compared year-long daily mean TDM-based T_{r_stand} (T_{r_TDM}) values calculated using the novel calibration equation and the original Granier equation in 2018, as well as the monthly mean T_{r_stand} values in 2010–2017 estimated by the STWB (T_{r_STWB}) (Fig. 7; Suppl. Material Table S2). Daily T_{r_stand} values were enhanced using the novel equation; the annual total T_r values calculated using the novel equation and the original equation were 593 and 229 mm year^{-1}, respectively. The relationship between the monthly T_{r_stand} value and meteorological factors suggests that T_{r_stand} at this site was mainly limited by VPD. The relationship between R_s and T_{r_stand} was statistically significant only when estimated using the original equation ($p < 0.001$). T_{r_TDM} estimated using the novel equation, and T_{r_STWB}, were not statistically significantly related to R_s ($p = 0.095$ and 0.053, respectively). The relationship between VPD and T_{r_stand} was statistically significant for all three estimates (all $p < 0.05$). Despite the inconsistency between the monthly mean T_{r_STWB} and T_{r_TDM} values obtained using the novel equation in December–April (i.e., winter to early spring), we did not observe a significant difference between these values over the year (paired t-test, $p > 0.05$). At the study site, snow in the wintertime and snowmelt in the late winter and early spring can delay Q and cause an increase in Q in March–April, resulting in underestimation of T_{r_STWB} values in March–April (Momiyama et al. 2019). This underestimation may be responsible for the sudden increase in T_{r_STWB} from April to May. The difference between T_{r_TDM} obtained using the novel equation and T_{r_STWB} was not statistically significant in May–November, i.e., excluding December–April (paired t-test, $p = 0.84$), verifying the validity of the TDM using the novel calibration equation.

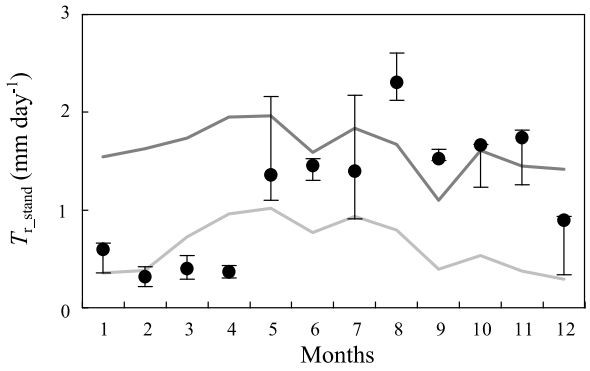

Fig. 7. Daily mean stand transpiration (T_{r_stand}) calculated by the novel calibration equation (dark gray line) and original Granier equation (light gray line) in 2018. Medians (closed circles) of monthly mean T_{r_stand} in 2010–2017 estimated by the short-term water budget method (STWB: Eq. (9)) are also shown. Error bars denote the range of the two middle quartiles of the data.

4. Discussion

4.1. Overview

We hypothesized that the accuracy of J_S and A_{S_stand} estimates is a critical factor in successfully estimating T_{r_stand} values using TDM. A_{S_stand} values are typically estimated by integrating A_{S_tree} over the whole stand, with individual values derived from the species-specific allometric relationship between DBH and A_{S_tree} within a number of sampled trees. In *Cr. japonica*, it is difficult to assess A_{S_tree}, i.e., the

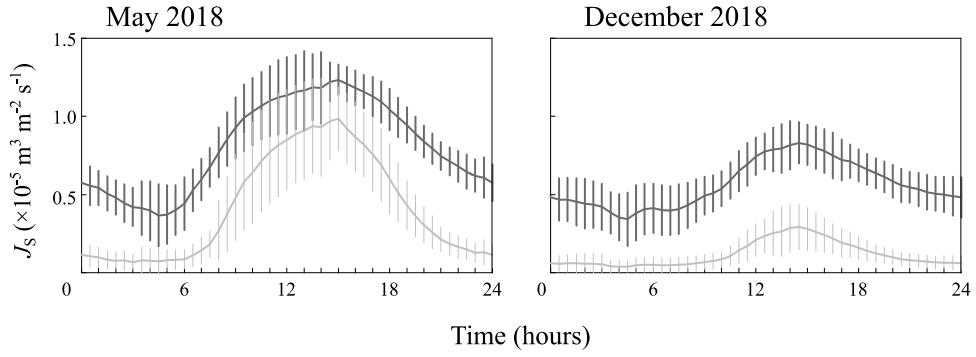

Fig. 6. Monthly mean diurnal courses of stand mean sap flux density (J_S) calculated using the novel species-specific calibration equation (dark gray lines) and original Granier calibration equation (light gray lines). May and December 2018 were the months with maximum and minimum monthly mean daily transpiration in 2018, respectively. Vertical bars indicate two SDs.

hydroactive zone in the stem cross-section, due to the unclear transition zone that is impervious to water between the sapwood and the heartwood, i.e., the white zone. Based on an analysis of 16 samples, we found that simple color identification of A_{S_tree} from apparent sapwood and heartwood had little effect on A_{S_stand} estimation, and in turn, T_{r_stand} estimation. This finding indicates that J_S is a strong determinant of accurate T_{r_stand} estimates. Despite the difficulty in detecting the white zone, a distinct color difference between apparent sapwood and heartwood in *Cr. japonica* stem cross-sections allows assessment of A_{S_tree} with comparative ease; the appropriate determination of A_{S_tree} in trees with an indistinct boundary between sapwood and heartwood, such as *Ch. obtusa*, another popular plantation species in Japan, requires more technically difficult examinations (Saito et al. 2015).

Correct estimation of J_S may depend on the accuracy of conversion of F_d from K and evaluation of radial variation in F_d. The results of our error analyses indicated that the species-specific parameters α and β in the K–F_d conversion equation were the most important determining factors in T_{r_stand} value estimates (Fig. 5). Many previous studies (Steppe et al. 2010, Sun et al. 2012, Paudel et al. 2013, Fuchs et al. 2017, Peters et al. 2018, Flo et al., 2019) have reported significant underestimation of actual F_d values when using the original Granier parameters, which implies its impact on estimates of larger-scale T_r. Our investigation confirmed these findings and also revealed that failure to evaluate the radial variation in F_d (Fig. 4) can be caused by the original Granier equation, further affecting T_{r_stand} estimates.

4.2. Species-specific calibration experiments

To improve the accuracy of the K–F_d conversion equation, laboratory calibration experiments are required to obtain novel species-specific parameters for the equation. Freshly cut logs or stem segments are typically used for these calibration experiments (see Fig. 2 in Steppe et al. 2010). When water is provided to the entire surface of the stem segment, there may be radial and azimuthal variation in F_d over the stem cross-section, making it difficult to evaluate the F_d corresponding to sapflow velocity in the vicinity of the probe (Steppe et al. 2010, Iida et al. 2020). Therefore, in this study we used cut sapwood segments, which allowed us to target F_d measured directly by the probe (Fig. 1a).

Although most previous calibration experiment studies have used positive pressure to generate water flow through the stem segments (e.g., de Oliveira Reis et al. 2006, Herbst et al. 2007, Hubbard et al. 2010, Steppe et al. 2010, Paudel et al. 2013), a few studies have used negative pressure as a driving force for artificial sapflow (Bush et al. 2010, Hultine et al. 2010, Schmidt-Walter et al. 2014, Fuchs et al. 2017) (Table S1). Each application of positive or negative pressure can become a potential source of error: water leakage and air entry for positive and negative pressure, respectively. Fuchs et al. (2017) mentioned that water leakage in experiments with positive pressure could decrease ΔT values and increase measured F_d values as a result of evaporative cooling on the stem surface, and that air entry in experiments with negative pressure could increase ΔT values and decrease measured F_d values as a result of xylem conduit drying and reduced heat conduction. Thus, underestimation of actual F_d values appears more likely in experiments under negative pressure than in those that use positive pressure or in field measurements. However, our analyses (Table S1) confirmed that there was no tendency to underestimate or overestimate F_d under negative and positive pressure, respectively. Furthermore, as Fuchs et al. (2017) also implied, studies have frequently reported underestimation of F_d values using the original Granier equation, which was developed from experiments using positive pressure, implying no clear relationship between F_d measurement and pressure type in the experiments. In the present study, we sealed the sides of the cut sapwood segments with silicon sealant to prevent air entry through the sides, and the force driving sapflow was intrinsically negative pressure. Thus, we consider that use of negative pressure generated by a vacuum pump is best for calibration experiments, and accordingly we examined the relationship between K_{min} in the calibration experiments listed in Table S1 and β in the conversion equation using only data acquired under negative pressure (Fig. 3).

Lu et al. (2004) were the first to suggest the need for calibration experiments to overcome deviations in TDM sensor design from the original Granier design, as well as variations in species-specific wood anatomical traits. Since then, TDM calibration equations have been tested in various experiments with a wide range of species and wood porosities, resulting in a large variety of species-specific calibration parameters, α and β, for Eq. (2) (Table S1). Thus, the mechanisms related to, for example, differences in variable-length probes (James et al. 2002, McCulloh et al. 2007) and differences in wood porosity among ring-porous, diffuse-porous, and conifer species (Bush et al. 2010, Sun et al. 2012, Xie and Wan 2018, Flo et al. 2019) are likely to affect determination of these parameters, but remain controversial.

The calibration curves (F_d as a function of K) obtained in this study and most previous studies produced higher F_d values for a given K than the original Granier curve (cf. Fig. 4 in Peters et al. 2018). F_d values estimated using species-specific calibrated parameters are generally higher than those proposed by Granier due to the steeper calibration curve, i.e., the larger value of β. In this case, the calibrated F_d becomes higher than the original curve-estimated value in the larger K domain, whereas the F_d calibrated in this study was higher (lower) in the lower (larger) K domain due to the gentle curve (i.e., the lowest β that we have ever obtained; Table S1 and Fig. 2). Thus, next we will discuss the very low β value obtained in this study, to answer the question regarding which factors determine the value of β.

A larger β value means a smaller amount of heat transportation (i.e., a smaller change in K) at a larger rate of sapflow. Thus, in sapwood with a large β value, sapflow has poor heat transportation efficiency, representing sapwood with a small proportion of water-filled areas over the cross-section and therefore a large wood density. A recent literature review (Peters et al. 2018) revealed that steeper calibration curves, which are assumed to have larger β, appeared in denser wood types, particularly ring-porous woody species.

However, contrary to expectations, our analyses using Table S1 found no significant relationships between β and either wood density or wood anatomy type. According to Fuchs et al. (2017), we hypothesized that relationships between β and sapwood characteristics would be distorted by experimental design effects such as limited ranges of K and F_d data for curve-fitting. The lower range of induced F_d and the corresponding K in each experiment may result in lower estimates of β because a power-law function cannot depict a steep curve pattern in such a limited data range. Fuchs et al. (2017) observed lower values of β (<1.0) in experiments using *Acer*, which had the lowest range of induced F_d. In our study, we examined relationships between maximum values of K (K_{max}) and K_{min} in each calibration experiment and β using data acquired only under negative pressure (Table S1); we used $\log_{10}K_{min}$ instead of K_{min} for this analysis due to the emphasis on differences in such very small K_{min} values between the previous experiments. As expected, this approach resulted in weak and moderately positive correlations between β and K_{max} ($R^2 = 0.27$, $p = 0.049$) and $\log_{10}K_{min}$ (Fig. 3; $R^2 = 0.47$, $p < 0.005$), respectively, confirming the demonstration by Hölttä et al. (2015) that TDM-based estimates of F_d are biased under low F_d conditions, at low sapwood thermal diffusivity.

Despite the minor situation, we found that the original Granier curve had higher predictive power at relatively high F_d values compared to the novel calibration curve (Fig. 2). Therefore, if TDM users simply require enhanced K–F_d conversion, we recommend applying a second-order polynomial of K (e.g., Herbst et al. 2008) or a two-step curve with two different combinations of α and β.

4.3. Corrected stand-scale transpiration and its effect on transpiration characteristics

Note that the novel K–F_d conversion equation modified radial

variation in F_d within individual trees (Fig. 4) by improving the evaluation of F_d in the lower K and F_d domains (Fig. 2), inducing an impact on correct T_{r_stand} estimates. For example, ratios of F_d at a depth of 20–40 mm to a depth of 0–20 mm (R_F) for conifers were 0.60 for *Pinus echinata* (Renninger and Schäfer 2012) and 0.41 for *Pinus taeda* (Phillips et al. 1996). Previous studies have estimated the R_F of *Cr. japonica* to be 0.37–0.78 (Kumagai et al. 2005a, 2007, Shinohara et al. 2013) and we obtained a value of 0.61 using the original Granier curve (Fig. 4); these findings appear plausible for conifers. By contrast, the novel calibration curve increased the value to 0.85 (Fig. 4), which is appreciably higher than ever recorded. Although the enhanced F_d obtained in the lower K domain may be peculiar to *Cr. japonica*, it would be reasonable for high sapflow rates to occur at greater sapwood depths; failure to correctly measure F_d at greater sapwood depth should be a significant source of error in T_{r_stand} estimates for *Cr. japonica*.

Further effects of the improved capacity for estimating low F_d should be provided based on T_{r_stand} estimates in low-F_d periods, i.e., nighttime and winter at daily and yearly time scales, respectively (Fig. 6). Nighttime F_d can be assumed to be nighttime water recharge into the stem (e.g., Kumagai et al. 2009) and/or actual nighttime T_r (e.g., Dawson et al. 2007), which are, in practice, difficult to differentiate. Peters et al. (2018) suggested that for conifers, although nighttime T_r is much smaller than daytime T_r, the water amount of nighttime T_r contributes appreciably to the annual water budget of forest stands. In *Cr. japonica*, because ~33% of transpired water is extracted from water stored in the stem sapwood (Kumagai et al. 2009), it is reasonable to assume that enhanced nighttime F_d and J_S (Fig. 6) should be exclusively attributed to nighttime water recharge. Likewise, it is thought that enhanced F_d in winter (Fig. 6) is plausible due to *Cr. japonica* maintaining photosynthetic activity and stomatal openness during winter (Kumagai et al. 2008).

Oishi et al. (2008) proposed determination criteria for ΔT_{max} (Eq. (3)) using VPD as a major driver of day-long sapflow, and demonstrated that it successfully increased both nighttime and daytime F_d values, resulting in TDM-based ET (i.e., $T_r + I_C$) similar to EC-measured ET. Notably, using the novel calibration curve in this study had the same effect as their method: to increase diurnal changes in F_d via searching for when zero-flow conditions (ΔT_{max}) occur (cf. Fig. 3 in Oishi et al. 2008 and Fig. 6 in this study). Thus, despite the importance of F_d modification by applying an appropriate zero-flow condition assumption (Peters et al. 2018), we did not examine how determining ΔT_{max} affects F_d calculations and the resulting T_{r_stand} estimates in this study. It should also be noted that signal (K) dampening caused by long-term probe installation would be a significant source of error when the TDM is applied to long-term T_r measurements (Peters et al. 2018), although we did not assume it problematic in our study site.

Using the novel K–F_d conversion equation, as a result of increasing nighttime and winter F_d, year-long daily T_{r_TDM} estimated by the original Granier equation was enhanced (Fig. 7). Considering the uncertainty in T_{r_STWB} during winter, on a monthly basis, year-long T_{r_TDM} obtained via the novel equation may show good agreement with T_{r_STWB}, implying the validity of the T_{r_TDM} estimates obtained using the novel equation. We obtained the multiplier 2.59 for the correct T_{r_stand} estimation from T_{r_TDM} using the original equation by dividing the annual novel equation T_{r_TDM} (593 mm year^{-1}) by the original equation value, 229 mm year^{-1}. The values estimated by this original equation are comparable to the uncalibrated annual transpiration of *Cr. japonica* reported in other studies, of 359 mm in southwestern Japan (Kumagai et al. 2014) and 122 mm in Taiwan (Laplace et al. 2017). Applying the multiplier 2.59 obtained in this study to a *Cr. japonica* forest watershed in southwestern Japan (Kumagai et al. 2014, Shimizu et al. 2015) increased the T_{r_TDM} estimate from 359 to 930 mm year^{-1}, a value comparable to the EC-measured water vapor flux of ca. 850 mm year^{-1}. Furthermore, the increase in T_{r_TDM} caused by the multiplier increased the TDM-based ET, from 911 to 1482 mm year^{-1}, making it consistent with the ET estimated by annual P_r minus annual Q which was equal to 1150-1400 mm year^{-1}.

Although the novel species-specific equation was not developed at a forest site, this case also demonstrates a strong need for novel species-specific calibration when using TDM for accurate T_{r_stand} and forest water balance.

A further defect caused by omitting the novel species-specific calibration may occur when individual tree T_r estimates are used to quantify T_r characteristics, mainly including canopy stomatal conductance (g_s: mmol m^{-2} leaf s^{-1}) (e.g., Pataki and Oren 2003), which can characterize environmental control of the canopy T_r and stomatal behavior. Generally, g_s is calculated from the inverted form of the Penman–Monteith equation (see Kumagai et al. 2008, 2009), and is related to environmental factors as $g_s = g_{sref} - m \ln(\mathrm{VPD})$ (Oren et al. 1999), where g_{sref} is the reference value of g_s (i.e., the value of g_s at VPD = 1 kPa), and m represents the sensitivity of g_s to VPD (i.e., $\partial g_s/\partial \ln \mathrm{VPD}$). Note that the proportionality $m/g_{sref} \approx 0.6$ results from the regulation of the minimum leaf water potential to prevent excessive xylem cavitation, and that a value of less than 0.6 denotes less strict stomatal regulation for dropping leaf water potential (Oren et al. 1999). In the same tree species (*Cr. japonica*), Kumagai et al. (2008) reported 35–55 mmol m^{-2} leaf s^{-1} and 0.25–0.49 for g_{sref} and m/g_{sref}, respectively. Using the original Granier curve, the *Cr. japonica* trees used in this study had g_{sref} values (~65 mmol m^{-2} leaf s^{-1}) comparable to those previously reported, but significantly lower proportionality (~0.12), which implies much less stomatal sensitivity to atmospheric evaporative demand, probably due to lower VPD throughout the year at this study site.

However, the novel species-specific calibration revised and considerably increased the values of g_{sref} and m/g_{sref} estimated by the original Granier curve to 200 mmol m^{-2} leaf s^{-1} and 0.31, respectively, implying critical misinterpretation of canopy stomatal behavior if the species-specific calibration equation is neglected. This finding may further reveal that previous TDM-based estimates of stomatal conductance parameters have been greatly underestimated. A retrospective investigation also demonstrated that porometric estimates of g_{sref} and m/g_{sref} were clearly higher than TDM estimates (cf. Tables 1 and 2 in Oren et al. 1999).

5. Conclusion

In this study, we showed that for TDM-based T_{r_stand} estimates, the calibrated conversion equation for heat-tracer-derived F_d values should be formulated for each tree species, because there have been significant underestimations of T_{r_stand} in most cases when using the original TDM equation. Although the present study dealt with a single popular plantation species, our findings are important with respect to the effects of novel species-specific calibration on both quantitative and qualitative analyses of tree water and the stand-scale water balance when using TDM. More extensive and technically advanced experiments are required to obtain effective information on how to apply TDM to more complex forests with a large variety of tree species.

Declaration of Competing interest

The authors declare that they have no known competing financial interests or personal relationships that could have appeared to influence the work reported in this paper.

Acknowledgments

Funding for this work was provided by the Kanagawa Prefectural Government, Japan, as part of the project on 'Forest, soil, and water resource conservation in the western Kanagawa reservoir area.'

The authors thank the staff of the Kanagawa Prefectural Government for logistical support to conduct observations throughout the Oborasawa Experimental Watershed (OEW). Members of the Laboratory of Forest Hydrology and Erosion Control Engineering (The University of Tokyo) also provided logistical support.

Supplementary materials

Supplementary material associated with this article can be found, in the online version, at doi:10.1016/j.agrformet.2021.108356.

References

Bladon, K.D., Silins, U., Landhäusser, S.M., Lieffers, V.J., 2006. Differential transpiration by three boreal tree species in response to increased evaporative demand after variable retention harvesting. Agric. For. Meteorol. 138, 104–119.

Brooks, J.R., Barnard, H.R., Coulombe, R., McDonnell, J.J., 2010. Ecohydrologic separation of water between trees and streams in a Mediterranean climate. Nature Geosci. 3, 100–104.

Burgess, S.S.O., Adams, M.A., Turner, N.C., Beverly, C.R., Ong, C.K., Khan, A.A.H., Bleby, T.M., 2001. An improved heat pulse method to measure low and reverse rates of sap flow in woody plants. Tree Physiol. 21, 589–598.

Bush, S.E., Hultine, K.R., Sperry, J.S., Ehleringer, J.R., 2010. Calibration of thermal dissipation sap flow probes for ring- and diffuse-porous trees. Tree Physiol. 30, 1545–1554.

Čermák, J., Deml, M., Penka, M., 1973. A new method of sap flow rate determination in trees. Biol. Plant. 15, 171–178.

Dawson, T.E., Burgess, S.S.O., Tu, K.P., Oliveira, R.S., Santiago, L.S., Fisher, J.B., Simonin, K.A., Ambrose, A.R., 2007. Nighttime transpiration in woody plants from contrasting ecosystems. Tree Physiol. 27, 561–575.

Delzon, S., Sartore, M., Granier, A., Loustau, D., 2004. Radial profiles of sap flow with increasing tree size in maritime pine. Tree Physiol. 24, 1285–1293.

Egusa, T., Kumagai, T., Oda, T., Gomi, T., Ohte, N., 2019. Contrasting patterns in the decrease of spatial variability with increasing catchment area between stream discharge and water chemistry. Water Resour. Res. 55, 7419–7435.

Ewers, B.E., Gower, S.T., Bond-Lamberty, B., Wang, C.K., 2005. Effects of stand age and tree species on canopy transpiration and average stomatal conductance of boreal forests. Plant Cell Environ. 28, 660–678.

Flo, V., Martinez-Vilalta, J., Steppe, K., Schuldt, B., Poyatos, R., 2019. A synthesis of bias and uncertainty in sap flow methods. Agric. For. Meteorol. 271, 362–374.

Fuchs, S., Leuschner, C., Link, R., Coners, H., Schuldt, B., 2017. Calibration and comparison of thermal dissipation, heat ratio and heat field deformation sap flow probes for diffuse-porous trees. Agric. For. Meteorol. 244-245, 151–161.

Granier, A., 1987. Evaluation of transpiration in a Douglas-fir stand by means of sap flow measurements. Tree Physiol. 3, 309–320.

Herbst, M., Roberts, J.M., Rosier, P.T.W., Gowing, D.J., 2007. Seasonal and interannual variability of canopy transpiration of a hedgerow in southern England. Tree Physiol. 27, 321–333.

Herbst, M., Rosier, P.T.W., Morecroft, M.D., Gowing, D.J., 2008. Comparative measurements of transpiration and canopy conductance in two mixed deciduous woodlands differing in structure and species composition. Tree Physiol. 28, 959–970.

Hölttä, T., Linkosalo, T., Riikonen, A., Sevanto, S., Nikinmaa, E., 2015. An analysis of Granier sap flow method, its sensitivity to heat storage and a new approach to improve its time dynamics. Agric. For. Meteorol. 211-212, 2–12.

Hubbard, R.M., Stape, J., Ryan, M.G., Almeida, A.C., Rojas, J., 2010. Effects of irrigation on water use and water use efficiency in two fast growing *Eucalyptus* plantations. Forest Ecol. Manag. 259, 1714–1721.

Hultine, K.R., Nagler, P.L., Morino, K., Bush, S.E., Burtch, K.G., Dennison, P.E., Glenn, E. P., Ehleringer, J.R., 2010. Sap flux-scaled transpiration by tamarisk (*Tamarix* spp.) before, during and after episodic defoliation by the saltcedar leaf beetle (*Diorhabda carinulata*). Agric. For. Meteorol. 150, 1467–1475.

Igarashi, Y., Katul, G.G., Kumagai, T., Yoshifuji, N., Sato, T., Tanaka, N., Tanaka, K., Fujinami, H., Suzuki, M., Tantasirin, C., 2015. Separating physical and biological controls on long-term evapotranspiration fluctuations in a tropical deciduous forest subjected to monsoonal rainfall. J. Geophys. Res. Biogeosci. 120, 1262–1278.

Iida, S., Shimizu, T., Shinohara, Y., Takeuchi, S., Kumagai, T., 2020. The Necessity of Sensor Calibration for the Precise Measurement of Water Fluxes in Forest Ecosystems. In: Levia, D., Carlyle-Moses, D., Iida, S., Michalzik, B., Nanko, K., Tischer, A. (Eds.), Forest-Water Interactions. Springer, Cham, Switzerland, pp. 29–54.

James, S.A., Clearwater, M.J., Meinzer, F.C., Goldstein, G., 2002. Heat dissipation sensors of variable length for the measurement of sap flow in trees with deep sapwood. Tree Physiol. 22, 277–283.

Jasechko, S., Sharp, Z.D., Gibson, J.J., Birks, S.J., Yi, Y., Fawcett, P.J., 2013. Terrestrial water fluxes dominated by transpiration. Nature 496, 347–350.

Kelliher, F.M., Leuning, R., Raupach, M.R., Schulze, E.D., 1995. Maximum conductances for evaporation from global vegetation types. Agric. For. Meteorol. 73, 1–16.

Komatsu, H., Shinohara, Y., Kume, T., Tsuruta, K., Otsuki, K., 2016. Does measuring azimuthal variations in sap flux lead to more reliable stand transpiration estimates? Hydrol. Processes 30, 2129–2137.

Kumagai, T., Aoki, S., Nagasawa, H., Mabuchi, T., Kubota, K., Inoue, S., Utsumi, Y., Otsuki, K., 2005a. Effects of tree-to-tree and radial variations on sap flow estimates of transpiration in Japanese cedar. Agric. For. Meteorol. 135, 110–116.

Kumagai, T., Nagasawa, H., Mabuchi, T., Ohsaki, S., Kubota, K., Kogi, K., Utsumi, Y., Koga, S., Otsuki, K., 2005b. Sources of error in estimating stand transpiration using allometric relationships between stem diameter and sapwood area for *Cryptomeria japonica* and *Chamaecyparis obtusa*. Forest Ecol. Manag. 206, 191–195.

Kumagai, T., Aoki, S., Shimizu, T., Otsuki, K., 2007. Sap flow estimates of stand transpiration at two slope positions in a Japanese cedar forest watershed. Tree Physiol. 27, 161–168.

Kumagai, T., Tateishi, M., Shimizu, T., Otsuki, K., 2008. Transpiration and canopy conductance at two slope positions in a Japanese cedar forest watershed. Agric. For. Meteorol. 148, 1444–1455.

Kumagai, T., Aoki, S., Otsuki, K., Utsumi, Y., 2009. Impact of stem water storage on diurnal estimates of whole-tree transpiration and canopy conductance from sap flow measurements in Japanese cedar and Japanese cypress trees. Hydrol. Processes 23, 2335–2344.

Kumagai, T., Tateishi, M., Miyazawa, Y., Kobayashi, M., Yoshifuji, N., Komatsu, H., Shimizu, T., 2014. Estimation of annual forest evapotranspiration from a coniferous plantation watershed in Japan (1): Water use components in Japanese cedar stands. J. Hydrol. 508, 66–76.

Laplace, S., Komatsu, H., Tseng, H., Kume, T., 2017. Difference between the transpiration rates of Moso bamboo (*Phyllostachys pubescens*) and Japanese cedar (*Cryptomeria japonica*) forests in a subtropical climate in Taiwan. Ecol. Res. 32, 835–843.

Linsley, R.K., Kohler, M.A., Paulhus, J.L.H., 1958. Hydrology for engineers. McGraw-Hill Book, New York.

Lu, P., Urban, L., Zhao, P., 2004. Granier's thermal dissipation probre (TDP) method for measuring sap flow in trees: theory and practice. Acta Bot. Sin. 46, 631–646.

Ma, C., Luo, Y., Shao, M., Li, X., Sun, L., Jia, X., 2017. Environmental controls on sap flow in black locust forest in Loess Plateau, China. Sci. Rep. 7, 1–12.

Mackay, D.S., Ahl, D.E., Ewers, B.E., Gower, S.T., Burrows, S.N., Samanta, S., Davis, K.J., 2002. Effects of aggregated classifications of forest composition on estimates of evapotranspiration in a northern Wisconsin forest. Global Change Biol. 8, 1253–1265.

Marshall, D.C., 1958. Measurement of Sap Flow in Conifers by Heat Transport. Plant Physiol. 33, 385–396.

Mcculloh, K.A., Winter, K., Meinzer, F.C., Garcia, M., Aranda, J., Lachenbruch, B., 2007. A comparison of daily water use estimates derived from constant-heat sap-flow probe values and gravimetric measurements in pot-grown saplings. Tree Physiol. 27, 1355–1360.

Momiyama, H., Kumagai, T., Egusa, T., 2019. Reproducing monthly evapotranspiration from a coniferous plantation watershed in Japan. J. For. Res. 24, 197–200.

Nadezhdina, N., Vandegehuchte, M.W., Steppe, K., 2012. Sap flux density measurements based on the heat field deformation method. Trees 26, 1439–1448.

Nakada, R., Fujisawa, Y., Hirakawa, Y., 1999. Soft X-ray observation of water distribution in the stem of *Cryptomeria japonica* D. Don I: General description of water distribution. J. Wood Sci. 45, 188–193.

Nobuchi, T., Harada, H., 1983. Physiological features of the "white zone" of sugi (*Cryptomeria japonica* D. Don): Cytological structure and moisture content. Mokuzai Gakkaishi 29, 824–832.

Oda, T., Suzuki, M., Egusa, T., Uchiyama, Y., 2013. Effect of bedrock flow on catchment rainfall-runoff characteristics and the water balance in forested catchments in Tanzawa Mountains. Japan. Hydrol. Processes 27, 3864–3872.

Oishi, A.C., Oren, R., Stoy, P.C., 2008. Estimating components of forest evapotranspiration: A footprint approach for scaling sap flux measurements. Agric. For. Meteorol. 148, 1719–1732.

de Oliveira Reis, F., Campostrini, E., de Sousa, E.F., e Silva, M.G., 2006. Sap flow in papaya plants: laboratory calibrations and relationships with gas exchanges under field conditions. Sci. Hortic. 110, 254–259.

Oren, R., Sperry, J.S., Katul, G.G., Pataki, D.E., Ewers, B.E., Phillips, N., Schäfer, K.V.R., 1999. Survey and synthesis of intra- and interspecific variation in stomatal sensitivity to vapour pressure deficit. Plant Cell Environ. 22, 1515–1526.

Pataki, D.E., Oren, R., 2003. Species differences in stomatal control of water loss at the canopy scale in a mature bottomland deciduous forest. Adv. Water Res. 26, 1267–1278.

Paudel, I., Kanety, T., Cohen, S., 2013. Inactive xylem can explain differences in calibration factors for thermal dissipation probe sap flow measurements. Tree Physiol. 33, 986–1001.

Peters, R.L., Fonti, P., Frank, D.C., Poyatos, R., Pappas, C., Kahmen, A., Carraro, V., Prendin, A.L., Schneider, L., Baltzer, J.L., Baron-Gafford, G.A., Dietrich, L., Heinrich, I., Minor, R.L., Sonnentag, O., Matheny, A.M., Wightman, M.G., Steppe, K., 2018. Quantification of uncertainties in conifer sap flow measured with the thermal dissipation method. New Phytol. 219, 1283–1299.

Phillips, N., Oren, R., Zimmermann, R., 1996. Radial patterns of xylem sap flow in non-, diffuse- and ring-porous tree species. Plant Cell Environ. 19, 983–990.

Poyatos, R., Granda, V., Molowny-Horas, R., Mencuccini, M., Steppe, K., Martínez-Vilalta, J., 2016. SAPFLUXNET: Towards a global database of sap flow measurements. Tree Physiol. 36, 1449–1455.

Renninger, H.J., Schäfer, K.V.R., 2012. Comparison of tissue heat balance- and thermal dissipation-derived sap flow measurements in ring-porous oaks and a pine. Front. Plant Sci. 3, 103.

Saito, T., Yamamoto, K., Komatsu, M., Matsuda, H., Yunohara, S., Komatsu, H., Tateishi, M., Xiang, Y., Otsuki, K., Kumagai, T., 2015. Using airborne LiDAR to determine total sapwood area for estimating stand transpiration in plantations. Hydrol. Processes 29, 5071–5087.

Schmidt-Walter, P., Richter, F., Herbst, M., Schuldt, B., Lamersdorf, N.P., 2014. Transpiration and water use strategies of a young and a full-grown short rotation coppice differing in canopy cover and leaf area. Agric. For. Meteorol. 195-196, 165–178.

Shimizu, T., Kumagai, T., Kobayashi, M., Tamai, K., Iida, S., Kabeya, N., Ikawa, R., Tateishi, M., Miyazawa, Y., Shimizu, A., 2015. Estimation of annual forest evapotranspiration from a coniferous plantation watershed in Japan (2): Comparison

of eddy covariance, water budget and sap-flow plus interception loss. J. Hydrol. 522, 250–264.
Shinohara, Y., Tsuruta, K., Ogura, A., Noto, F., Komatsu, H., Otsuki, K., Maruyama, T., 2013. Azimuthal and radial variations in sap flux density and effects on stand-scale transpiration estimates in a Japanese cedar forest. Tree Physiol. 33, 550–558.
Steppe, K., De Pauw, D.J.W., Doody, T.M., Teskey, R.O., 2010. A comparison of sap flux density using thermal dissipation, heat pulse velocity and heat field deformation methods. Agric. For. Meteorol. 150, 1046–1056.
Sun, H., Aubrey, D.P., Teskey, R.O., 2012. A simple calibration improved the accuracy of the thermal dissipation technique for sap flow measurements in juvenile trees of six species. Trees 26, 631–640.
Sun, X., Onda, Y., Otsuki, K., Kato, H., Hirata, A., Gomi, T., 2014. The effect of strip thinning on tree transpiration in a Japanese cypress (*Chamaecyparis obtusa* Endl.) plantation. Agric. For. Meteorol. 197, 123–135.
Suzuki, M., 1985. Evapotranspiration estimates of forested watersheds in Japan using the short-time period water-budget method. J. Jpn. For. Soc. 67, 115–125.
Tateishi, M., Kumagai, T., Suyama, Y., Hiura, T., 2010. Differences in transpiration characteristics of Japanese beech trees, *Fagus crenata*, in Japan. Tree Physiol. 30, 748–760.
Wullschleger, S.D., Hanson, P.J., Todd, D.E., 2001. Transpiration from a multi-species deciduous forest as estimated by xylem sap flow techniques. Forest Ecol. Manag. 143, 205–213.
Xie, J., Wan, X., 2018. The accuracy of the thermal dissipation technique for estimating sap flow is affected by the radial distribution of conduit diameter and density. Acta Physiol. Plant. 40, 88. https://doi.org/10.1007/s11738-018-2659-y.
Zwieniecki, M.A., Melcher, P.J., Holbrook, N.M., 2001. Hydrogel control of xylem hydraulic resistance in plants. Science 291, 1059–1062.